

8526  
NACA TN 2942

0066189

TECH LIBRARY KAFB, NM

# NATIONAL ADVISORY COMMITTEE FOR AERONAUTICS

TECHNICAL NOTE 2942

PRESSURE DISTRIBUTIONS ABOUT FINITE WEDGES IN BOUNDED  
AND UNBOUNDED SUBSONIC STREAMS

By Patrick L. Donoughe and Ernst I. Prasse

Lewis Flight Propulsion Laboratory  
Cleveland, Ohio



Washington  
May 1953

AFMCC  
TECHNICAL LIBRARY  
AFL 2811



## NATIONAL ADVISORY COMMITTEE FOR AERONAUTICS

## TECHNICAL NOTE 2942

PRESSURE DISTRIBUTIONS ABOUT FINITE WEDGES IN BOUNDED  
AND UNBOUNDED SUBSONIC STREAMS

By Patrick L. Donoughe and Ernst I. Prasse

## SUMMARY

An analytical and experimental investigation on pressure distribution about wedges was initiated because of some problems encountered in transpiration cooling; the results obtained are of general interest and application. The analytical investigation of incompressible flow about finite wedges showed that decreasing the tunnel-wedge ratio (the tunnel-wedge ratio is defined as ratio of tunnel height to maximum wedge thickness) decreased the pressure coefficient at all chordwise locations; an increase in wedge angle with an unbounded stream (infinite tunnel-wedge ratio) caused a pressure coefficient increase in the forward region and decrease in the rear region of the wedge. It was also found that even for a wedge in an unbounded stream the region of applicability of the infinite wedge-type velocity distribution assumed in the solution of laminar boundary layer equations is approximated only within 10 percent for a limited leading-edge region. Additional calculations indicated that use of a theoretical instead of an experimental pressure distribution should be satisfactory for heat-transfer predictions for regions not unduly influenced by flow separation.

Comparison of theoretical and experimental pressure distributions about wedges in compressible subsonic flow showed poor agreement for a wedge angle of  $30^\circ$  and a tunnel-wedge ratio of 2.8, probably because of flow separation. For wedge angles from  $9^\circ$  to  $20^\circ$  and essentially unbounded streams (tunnel-wedge ratio of 100), the results from a simple mapping Kármán-Tsien method were in good agreement with experiment for Mach numbers to 0.700. A hodograph method predicted results in good agreement with experiment for an essentially unbounded stream, even for Mach numbers close to unity.

## INTRODUCTION

The question of the influence of the tunnel wall on the pressure distribution over a finite wedge arose in connection with some problems encountered in obtaining heat-transfer results for transpiration cooling. Prediction of the coolant flow emitted from a porous wedge, used as a test vehicle, necessitated knowledge of the pressure distribution about the reference solid wedge. This distribution was obtained by placing a  $30^\circ$  solid wedge with a 2-inch chord in the tunnel used for the porous wedge investigation. The resulting tunnel-wedge ratio was 2.8 where this ratio is defined as the ratio of the height of the tunnel to the maximum thickness of the wedge. Attempts were made to correlate the data with analytical solutions available in the literature.

In addition to the use for transpiration cooling analyses, wedges may be used as the leading section of compressor and turbine blades and wings, and are also useful in the solution of the laminar boundary layer equations. Experimental Mach number and pressure distributions obtained from interferometer measurements are given in references 1 and 2. A review of the different theories for the potential flow about wedges in an unbounded stream is also given in reference 1. The theoretical effects of compressibility may be obtained for subsonic flow by either the method of reference 3 or, if the incompressible pressure distribution is known, by use of Prandtl-Glauert or Kármán-Tsien corrections.

For laminar boundary layer solutions, the stream velocity in the potential flow is assumed to increase in proportion to some power of the distance from the leading edge. This type of velocity distribution is realized in the two-dimensional, incompressible flow about wedges infinite in the chordwise direction with an unbounded stream, that is, an infinite wedge with a tunnel-wedge ratio of infinity. Such boundary layer solutions are given in references 4 to 6; references 5 and 6 give solutions for porous surfaces with large temperature differences between the surface and the main stream. In actual practice, however, only finite wedges can be used. In addition, experiments would usually be conducted in a wind tunnel, so that the influence of the tunnel wall on the wedge pressure distribution is important. Hence, if results of boundary layer theory are to be correlated with experiment, it is necessary to have an estimate of the region on a finite wedge in a bounded stream where the infinite wedge-type flow assumed in this theory is approximately realized.

2805

In the present report, experimental pressure distributions were determined and flow visualization studies were made for the  $30^\circ$  wedge with a tunnel-wedge ratio of 2.8 and upstream Mach numbers of the order of 0.350. Theoretical and experimental pressure distributions for the  $30^\circ$  wedge were used to predict the heat transfer to the wedge by the methods of reference 7. Analytical pressure distributions for tunnel-wedge ratios from 2.8 to 170 and wedge angles from  $0^\circ$  to  $40^\circ$  were calculated for incompressible flow. The region of applicability of the infinite wedge-type pressure distribution for a finite wedge in a bounded stream was analyzed. Since no direct comparison of experimental and theoretical pressure distributions for upstream Mach numbers close to unity was found in the literature, a comparison of previously published experimental and theoretical results was also made.

## APPARATUS

### Wedge

For the present experimental investigation a  $30^\circ$  wedge was machined from Inconel stock. The wedge had no afterbody because of space limitations in the tunnel. Static-pressure taps (0.020-in. diam.) were drilled perpendicular to the surface at three different spanwise and various chordwise locations and connected to the ends of the wedge with drilled passages. Into these passages steel tubing was silver-soldered for attachment of the flexible tubing which led to the manometer board. Rods on each end of the wedge held it in place and acted as pivots for orienting the wedge at zero angle of attack. The geometry and pressure tap locations for the wedge are shown in table I. The resulting tunnel-wedge ratio for this configuration is 2.83. The pressures on the wedge were read differentially with the upstream static pressure, the manometer fluid being water. Pressure readings at different spanwise locations agreed within less than 1 percent for the same chordwise location.

### Test Facility

In the test facility, laboratory air passed successively through a standard A.S.M.E. orifice, a combustion chamber, a plenum chamber (where stagnation temperature and pressure were measured), and the test section and into the exhaust system. For the present investigation no fuel was added in the combustion chamber. The plenum chamber and tunnel sections are shown in figure 1. The inlet duct to the test section extended into the plenum chamber to insure a uniform velocity profile in

the test section. Care was taken in assembly of the entrance and test sections so that no protuberances existed in the flow passage.

The flow passage of the entrance and test sections downstream of the inlet duct was nominally 3 inches square with four outer walls spaced at  $3/8$  inch intervals to minimize heat loss for any high temperature work (see fig. 1). The 3-inch-square cross section was maintained for about 23 chord lengths (46 in.) upstream of the wedge. Stagnation pressure was also measured with a total-pressure probe about 8 chord lengths upstream of the wedge. This pressure probe was read differentially with a wall static tap  $4\frac{1}{2}$  chord lengths ahead of the wedge. The wall static pressure was also read absolutely, the manometer fluid being water for both the differential and absolute readings. These pressure readings were used to calculate the upstream Mach number.

### Flow Visualization

In an attempt to confirm the two-dimensionality of the flow about the wedge, flow visualization studies were made. In these studies hydrogen sulfide gas reacted with a mixture of glycerin and lead carbonate painted on the wedge and side walls. After the hydrogen sulfide was introduced through static taps on the wedge and side walls, its paths along the wedge and on the walls were observed as brown traces on a white background. More details of visualization methods for gas flow about turbine blades are reported in reference 8.

### TEST PROCEDURE

Pressure taps symmetrically located closest to the leading edge on either side of the wedge (see table I) were used to set the angle of attack to zero. When the pressures at these taps agreed within 0.1 inch of water, the pressure readings on the wedge were taken for the following upstream conditions:

| $M_0$ | $p_0$ ,<br>in. water abs | $p' - p_0$ ,<br>in. water | $T'$ ,<br>°R |
|-------|--------------------------|---------------------------|--------------|
| 0.266 | 435.0                    | 21.9                      | 560          |
| .286  | 466.9                    | 27.3                      | 552          |
| .328  | 421.7                    | 32.6                      | 560          |
| .403  | 444.2                    | 52.5                      | 558          |
| .464  | 513.0                    | 81.7                      | 555          |

Symbols are defined in the appendix.

## ANALYSIS

Analytical methods to determine the static-pressure distribution for flow about finite wedges are given. The static pressure on the wedge is incorporated in a pressure coefficient which is defined by

$$C_p \equiv \frac{p - p_0}{\frac{\rho_0 U_0^2}{2}} \quad (1)$$

For isentropic incompressible flow, the pressure coefficient is related to the velocity by

$$C_{p,i} = 1 - \left( \frac{U}{U_0} \right)^2 \quad (1a)$$

For isentropic compressible flow, the pressure coefficient is related to the Mach number by

$$C_p = \frac{2}{\gamma M_0^2} \left[ \left( \frac{1 + \frac{1}{2}(\gamma-1)M_0^2}{1 + \frac{1}{2}(\gamma-1)M^2} \right)^{\frac{\gamma}{\gamma-1}} - 1 \right] \quad (1b)$$

The pressure gradient in the direction of flow is given in dimensionless form by the Euler number which is defined by (ref. 9)

$$Eu \equiv - \frac{x}{\rho U^2} \frac{dp}{dx} = \frac{x}{U} \frac{dU}{dx} \quad (2)$$

The last equality results from Bernoulli's equation.

The usual corrections for the effects of compressibility (Prandtl-Glauert and Kármán-Tsien methods) which apply for subsonic flow are given; in addition, the theory of reference 3 for flow over a finite wedge in an unbounded stream is utilized.

## Incompressible Flow

Infinite wedge, unbounded stream. - For an infinite wedge in an unbounded stream, the velocity variation on the wedge surface is given by (ref. 4)

$$U = cx^m \quad (3)$$

Differentiation of equation (3) and use of equation (2) show that  $m \equiv Eu$ . By a conformal transformation of the region outside the wedge, it may be shown that the exponent  $m$  or the Euler number is related to the wedge angle by

$$Eu = \frac{\theta}{2\pi - \theta} \quad (4)$$

for

$$0 \leq \theta \leq \pi$$

This result has already been given in reference 10.

The velocity distribution given by equation (3) has been used extensively in solution of the laminar boundary layer equations under the assumption that the Euler number is constant for a given solution.

Finite wedge, bounded stream. - In actual practice, only finite wedges can be constructed and experiments with them would probably be conducted in a wind tunnel. Hence the pressure distribution about a finite wedge in a finite, bounded stream must be determined. For the case of incompressible flow about a finite wedge in a bounded stream, recourse is made to the mapping theorem of Schwarz and Christoffel for the theoretical approach. A general discussion of the Schwarz-Christoffel theorem is given in reference 11. To obtain the pressure distribution about a wedge centrally located in a rectangular tunnel, it is necessary to consider only the upper half of the wedge because of flow symmetry. The region to be analyzed is shown schematically in figure 2. The wedge is assumed to have an afterbody of infinite length to simplify the analysis. The theory, of course, precludes any separation of the flow. By a Schwarz-Christoffel transformation the boundary of the flow region of the physical or  $z$ -plane is transformed into the real axis of the  $\zeta$ -plane,  $z$  and  $\zeta$  being complex variables. The following points may be specified:

1. The leading edge E in the  $z$ -plane shall map into the point  $(t,0)$  in the  $\zeta$ -plane.
2. The trailing edge D in the  $z$ -plane shall map into the point  $(1,0)$  in the  $\zeta$ -plane.
3. The infinite point  $B_{\infty}C_{\infty}$  in the  $z$ -plane shall map into the point  $(0,0)$  in the  $\zeta$ -plane.
4. The infinite points  $A_{\infty}$  and  $F_{\infty}$  shall map into negative and positive infinity, respectively, in the  $\zeta$ -plane.

The transformation from the  $\zeta$ -plane to the  $z$ -plane for this configuration can be obtained from the theorem of Schwarz and Christoffel as

$$\frac{dz}{d\zeta} = \frac{S}{\zeta} \left( \frac{\zeta - 1}{\zeta - t} \right)^{\frac{\theta}{2\pi}} \quad (5)$$

where  $S$  and  $t$  are constants to be determined.

In the physical or  $z$ -plane the flow is from a source of output  $U_0 a/2$  at  $A_\infty$  to a sink of intake  $U_0 a/2$  at  $B_\infty$ . In the  $\zeta$ -plane this requires a sink of strength  $U_0 a/2\pi$  at the origin. The flow induced by the sink in the  $\zeta$ -plane is characterized by the complex potential

$$w = \frac{U_0 a}{2\pi} \ln \zeta \quad (6)$$

The complex velocity in the  $z$ -plane, being the derivative of the potential, is obtained from equations (5) and (6).

$$\frac{dw}{dz} = \frac{dw}{d\zeta} \frac{d\zeta}{dz} = \frac{U_0 a}{2\pi S} \left( \frac{\zeta - t}{\zeta - 1} \right)^{\frac{\theta}{2\pi}} \quad (7)$$

As  $\zeta \rightarrow \infty$  ( $F_\infty$  in the  $z$ -plane), the derivative of the potential must give the upstream velocity  $U_0$

$$\left( \frac{dw}{dz} \right)_{\zeta \rightarrow \infty} = U_0$$

and the limit of the term in parentheses in equation (7) is given by

$$\lim_{\zeta \rightarrow \infty} \left( \frac{\zeta - t}{\zeta - 1} \right)^{\frac{\theta}{2\pi}} = 1$$

so that  $S = a/2\pi$ . At  $\zeta = 0$  ( $B_\infty$  in the  $z$ -plane), continuity considerations require that  $\frac{dw}{dz} = \frac{U_0 a}{a - b}$ . Substitution of this value for the derivative and of  $\zeta = 0$  into equation (7) gives

$$t = \left( \frac{a/b}{a/b - 1} \right)^{\frac{2\pi}{\theta}} \quad (8)$$



Thus the constants  $S$  and  $t$  are determined as functions of the wedge angle and tunnel-wedge ratio.

The real velocity on the wedge surface is evaluated by obtaining the absolute value of  $dw/dz$  on the wedge surface. This surface corresponds to the segment DE (fig. 2) of the real axis of the  $\zeta$ -plane where  $\zeta = \alpha$ .

$$\begin{aligned}
 U = \left| \frac{dw}{dz} \right| &= U_0 \left| \frac{\alpha - t}{\alpha - 1} \right|^{\frac{\theta}{2\pi}} \\
 &= U_0 \left( \frac{t - \alpha}{\alpha - 1} \right)^{\frac{\theta}{2\pi}} \quad (9) \\
 &\text{for} \\
 &1 \leq \alpha \leq t
 \end{aligned}$$

Equation (1a) is used to find the pressure coefficient for a finite wedge in a bounded stream

$$\begin{aligned}
 C_{p,i} &= 1 - \left( \frac{t - \alpha}{\alpha - 1} \right)^{\frac{\theta}{\pi}} \quad (10) \\
 &\text{for} \\
 &1 \leq \alpha \leq t
 \end{aligned}$$

$C_{p,i}$  may be evaluated, therefore, when the relation between  $\alpha$  and  $x$  in the  $\zeta$ - and  $z$ -planes is established. This relation is obtained by numerical integration of equation (5) as follows.

Since the flow over the wedge surface in the  $z$ -plane, which maps into the segment DE of the real axis of the  $\zeta$ -plane, is of interest, points appropriately spaced between  $\alpha = 1$  and  $\alpha = t$  are chosen. On this segment,  $|z| = x$  and  $\zeta = \alpha$ ; so that from equation (5),

$$\frac{d(x/L)}{d\alpha} = - \frac{1}{L} \left| \frac{dz}{d\zeta} \right| = - \frac{S}{L\alpha} \left( \frac{\alpha - 1}{t - \alpha} \right)^{\frac{\theta}{2\pi}} = - \frac{1}{\pi} \frac{a}{b\alpha} \left( \frac{\alpha - 1}{t - \alpha} \right)^{\frac{\theta}{2\pi}} \sin \frac{\theta}{2} \quad (11)$$

from which

$$\frac{x}{L}(\alpha) = 1 - \frac{a \sin(\theta/2)}{b\pi} \int_1^\alpha \frac{1}{\alpha} \left( \frac{\alpha - 1}{t - \alpha} \right)^{\frac{\theta}{2\pi}} d\alpha \quad (12)$$

for

$$1 \leq \alpha \leq t$$

Then  $x/L$  may be obtained with the aid of equation (12) and the finite difference integration formula (ref. 12, p. 243).

$$\begin{aligned} \int_{\alpha_1}^{\alpha_1 + nh} \frac{1}{\alpha} \left( \frac{\alpha - 1}{t - \alpha} \right)^{\frac{\theta}{2\pi}} d\alpha &= nh \left[ 1 + \frac{n}{2} \Delta + \frac{n(2n-3)}{12} \Delta^2 + \frac{n(n-2)^2}{24} \Delta^3 + \right. \\ &\quad \left. \frac{n(6n^3 - 45n^2 + 110n - 90)}{720} \Delta^4 + \frac{n(2n^4 - 24n^3 + 105n^2 - 200n + 144)}{1440} \Delta^5 + \right. \\ &\quad \left. \frac{n(12n^5 - 210n^4 + 428n^3 - 4725n^2 + 7672n - 5040)}{60,480} \Delta^6 + \dots \right] \left[ \frac{1}{\alpha_1} \left( \frac{\alpha_1 - 1}{t - \alpha_1} \right)^{\frac{\theta}{2\pi}} \right] \end{aligned} \quad (13)$$

If accurate results are to be obtained from this numerical integration, the nature and behavior of the function  $d(x/L)/d\alpha$  must be known for  $1 \leq \alpha \leq t$ . In particular, for values of  $\alpha$  in the neighborhood of a maximum or minimum value of  $d(x/L)/d\alpha$ , it is necessary to use smaller values of  $n$  and  $h$  than those which may be used in other regions. At maximum or minimum values of  $d(x/L)/d\alpha$ ,  $d^2(x/L)/d\alpha^2$  must vanish. Differentiating equation (11) and equating this result to zero yield the quadratic equation in  $\alpha$

$$\frac{1}{\alpha} = \frac{\theta}{2\pi} \left[ \frac{t - 1}{(\alpha - 1)(t - \alpha)} \right] \quad (14)$$

If equation (14) has no real roots,  $d(x/L)/d\alpha$  has no maximum or minimum values. If equation (14) has real roots, say  $\alpha_2$  and  $\alpha_3$  with  $\alpha_2 \leq \alpha_3$ , then  $d(x/L)/d\alpha$  increases for  $1 \leq \alpha \leq \alpha_2$  to a maximum at  $\alpha = \alpha_2$ , decreases for  $\alpha_2 \leq \alpha \leq \alpha_3$  to a minimum at  $\alpha = \alpha_3$ , and finally increases

for  $\alpha_3 \leq \alpha < t$ , becoming infinite as  $\alpha \rightarrow t$ . Hence, for a given tunnel-wedge configuration,  $\alpha_2$  and  $\alpha_3$  may be determined from equation (14), if they exist, and appropriate values of  $n$  and  $h$  may be used in equation (13) to determine  $x/L$ .

For the corresponding Euler number distribution along the wedge, use of equations (2), (9), (11), and  $dU/dx = dU/d\alpha/dx/d\alpha$  yields

$$Eu = \frac{\frac{\theta}{2} (t - 1)}{\frac{a}{b} \sin \frac{\theta}{2}} \frac{x}{L} \frac{U}{U_0} \left[ \frac{\alpha}{(\alpha - 1)(t - \alpha)} \right] \quad (15)$$

Hence the Euler number may be calculated for each value of  $\alpha$  by use of the results from the finite-difference calculation. At the leading edge (the stagnation point), corresponding to  $\alpha = t$ , the right side of equation (15) becomes indeterminate. It can be shown, however, by use of L'Hospital's Rule that as  $\alpha$  approaches  $t$ , the Euler number approaches the value given by equation (4) for an infinite wedge of angle  $\theta$  in an unbounded stream.

An independent check of the velocities obtained by this mapping method was obtained for  $\theta = 30^\circ$  and  $a/b = 2.8$  by employment of a mechanical stream-filament method. This method uses steel wires for the streamlines and the orthogonal lines. Upon proper alinement of the wire network, the velocity ratio  $U/U_0$  is given by the ratio of the length of the rectilinear square upstream of the body to the length of the rectilinear square on the surface of the body. Details of the method are given in reference 13. The resulting flow pattern for the test configuration is shown in figure 3. Velocities obtained from this network agreed within 2 percent with those calculated from the mapping method.

Finite wedge, unbounded stream. - The flow about a finite wedge in an unbounded stream can be deduced in a manner similar to that used for the bounded stream. For this configuration employment of the theorem of Schwarz and Christoffel yields for the wedge surface

$$\frac{x}{L}(\alpha) = 1 - \frac{s}{L} \int_{-1}^{\alpha} \left( \frac{1 + \alpha}{1 - \alpha} \right)^{\frac{\theta}{2\pi}} d\alpha \quad (16)$$

for

$$-1 \leq \alpha \leq 1$$

and

$$U = U_0 \left( \frac{1 - \alpha}{1 + \alpha} \right)^{\frac{\theta}{2\pi}}$$

so that

$$C_{p,i} = 1 - \left( \frac{1 - \alpha}{1 + \alpha} \right)^{\frac{\theta}{\pi}} \quad (17)$$

for

$$-1 \leq \alpha \leq 1$$

and

$$Eu = \frac{\theta}{\pi} \frac{x/L}{s/L} \frac{U}{U_0} \frac{1}{1 - \alpha^2} \quad (18)$$

In this transformation,  $x/L = 0$  corresponds to  $\alpha = 1$ , that is,  $\frac{x}{L}(1) = 0$ , so that from equation (16)

$$\frac{s}{L} = \left[ \int_{-1}^1 \left( \frac{1 + \alpha}{1 - \alpha} \right)^{\frac{\theta}{2\pi}} d\alpha \right]^{-1}$$

For evaluation of this integral and for the integration of equation (16), the finite-difference formula (ref. 12, p. 243) is again used. As in the case of a finite wedge in a bounded stream, the Euler number given by equation (18) approaches the value given by equation (4) for an infinite wedge of angle  $\theta$  in an unbounded stream as the leading edge is approached ( $\alpha \rightarrow 1$ ).

A linearized theory for the pressure distribution for incompressible flow about a finite wedge in an unbounded stream is presented in appendix B of reference 1. The pressure coefficient on the wedge surface is given by

$$C_{p,i} = -\frac{\theta}{\pi} \ln \frac{x/L}{1 - x/L} \quad (19)$$

Because of the limitations of the linearized theory, the point of zero pressure coefficient is fixed at  $x/L = 0.5$  regardless of the wedge angle, as is seen by equation (19). Examination of equations (16) and (17), obtained by the mapping method, shows that  $C_{p,i} = 0$  does not always occur at  $x/L = 0.5$ , but its location will vary depending on the wedge angle.

### Compressible Flow

Several theoretical approaches have been used to account for the influence of compressibility on the pressure coefficient for appreciable subsonic Mach numbers (see ref. 14). With respect to ease of utilization, the simpler theories are the Prandtl-Glauert and Kármán-Tsien methods which correct the incompressible pressure coefficient for Mach number. The Prandtl-Glauert method gives

$$C_p = \frac{C_{p,i}}{\sqrt{1 - M_0^2}} \quad (20)$$

and the Kármán-Tsien method gives

$$C_p = \frac{C_{p,i}}{\sqrt{1 - M_0^2} + \frac{M_0^2}{1 + \sqrt{1 - M_0^2}} \frac{C_{p,i}}{2}} \quad (21)$$

Thus the pressure coefficient for compressible flow is obtainable if the upstream Mach number and the incompressible pressure coefficient are known.

Finite wedge, bounded stream. - The Prandtl-Glauert and Kármán-Tsien corrections are, strictly speaking, applicable for an unbounded stream, or at least where the interference from the tunnel wall is small. Qualitative estimates of the compressibility effects, on the other hand, may be obtained by use of these methods. The Kármán-Tsien method, rather than the Prandtl-Glauert method, was used to investigate compressibility effects on the experimental test configuration  $\theta = 30^\circ$ ,  $a/b = 2.8$ , since  $C_{p,i}$  is large over most of the wedge and the Kármán-Tsien correction is in better agreement with experiment in this range (ref. 14, p. 246).

Finite wedge, unbounded stream. - The pressure distribution for a finite wedge in an unbounded stream may be obtained quite readily by equations (19) and (20). The result has already been given in reference 1 as

$$C_p = - \frac{\theta}{\pi \sqrt{1 - M_0^2}} \ln \frac{x/L}{1 - x/L} \quad (22)$$

It is anticipated that equation (22) will become less valid when  $M_0$  is close to unity. In this case the solution from a hodograph method given in reference 3 also may be utilized. The series representation of  $x/L$  on the wedge surface given by equation (53) of reference 3 is, in the notation of the present report,

$$x/L = - 2N_0^{\frac{1}{3}} N^{\frac{2}{3}} \sum_{r=1}^{\infty} (-1)^r \left( \frac{r\pi}{v} \right) K_{\frac{2}{3}} \left( \frac{r\pi N}{v} \right) I_{-\frac{1}{3}} \left( \frac{r\pi N_0}{v} \right) \quad (23)$$

for

$$N > N_0 > 0$$

$$x/L = 1 + 2N_0^{\frac{1}{3}} N^{\frac{2}{3}} \sum_{r=1}^{\infty} (-1)^r \left( \frac{r\pi}{v} \right) K_{\frac{1}{3}} \left( \frac{r\pi N_0}{v} \right) I_{\frac{2}{3}} \left( \frac{r\pi N}{v} \right) \quad (24)$$

for

$$N_0 > N > 0$$

where

$r$  = summation index

$$\left. \begin{aligned} N_0 &= (2/3)(1 - M_0^2)^{\frac{3}{2}} \\ N &= (2/3)(1 - M^2)^{\frac{3}{2}} \\ v &= \frac{(\gamma + 1)}{2} \theta \end{aligned} \right\} \quad (25)$$

and  $I_p$  and  $K_p$  are modified Bessel functions of the first and second kinds, respectively. The modified Bessel function of the second kind  $K_p$  is related to  $I_p$  by (ref. 12, p. 317)

$$K_p(\arg) = \frac{\pi}{2} \frac{I_{-p}(\arg) - I_p(\arg)}{\sin p \pi}$$

The modified Bessel function of the first kind  $I_p$  is tabulated in reference 15, so that it and the modified Bessel function of the second kind  $K_p$  are obtainable.

Examination of equations (23) and (24) shows that equation (23) is for the front portion of the wedge, since here  $M^2 \leq M_0^2$  so that  $N \geq N_0$ ; equation (24) is for the rear portion, since there  $M^2 \geq M_0^2$  so that  $N_0 \geq N$ . With this in mind, equations (23) and (24) can be solved for  $x/L$  by assigning values  $N$ ,  $N_0$ , and  $v$  and calculating the modified Bessel functions over the range of  $r$ .

In the so-called transonic approximation, the pressure coefficient is approximated by the relation given in references 3, 16, and 17, which is, in the notation of the present report,

$$C_p = \frac{2}{\gamma+1} (M_0^2 - M^2) \quad (1c)$$

Since assigned values of  $N$  and  $N_0$  fix  $M$  and  $M_0$  by equation (25),  $C_p$  can be calculated by use of equation (1c) for the hodograph method for the finite wedge, unbounded stream. Thus  $C_p$  is calculable for the hodograph method, and by use of equation (22)  $C_p$  for linearized subsonic flow may be calculated. These calculations may then be used for comparison with the experimental pressure coefficients obtained from data in reference 1.

## RESULTS AND DISCUSSION

Analytical results of the incompressible flow about finite wedges will be presented and the effects of wedge angle and tunnel-wedge ratio will be discussed. An estimate will be made of the region of applicability of the infinite wedge-type flow (constant Euler number) assumed in boundary layer theory. Predictions of heat transfer to the  $30^\circ$  wedge for a tunnel-wedge ratio of 2.83 will also be given. The results of the flow visualization studies on the  $30^\circ$  test configuration as well as a comparison of analytical and experimental pressure distributions for this wedge

will be shown. Comparison between compressible theory and experimental pressure distributions of reference 1 will be made for subsonic flow.

### Analytical

Effect of wedge angle. - Pressure coefficients were calculated by use of equation (10) for incompressible flow ( $M_0 = 0$ ) about  $9^\circ$ ,  $15^\circ$ , and  $20^\circ$  wedge angles; the chordwise location corresponding to each coefficient was obtained by equation (12). The tunnel-wedge configurations are those for which experimental data are given in reference 1. For each of these configurations the tunnel-wedge ratio is sufficiently large that tunnel wall influence is relatively insignificant. The pressure distributions for finite wedges in an unbounded stream ( $a/b = \infty$ ) were also calculated using equations (17) and (16). These analytical results for incompressible flow about finite wedges are presented in figure 4 and table II. Figure 4(a) shows a plot of computed pressure coefficient against chordwise location for  $0^\circ \leq \theta \leq 40^\circ$ . Note that the location of the zero pressure coefficient moves downstream with increasing wedge angle. Figure 4(b), a cross plot of figure 4(a), shows the variation of the pressure coefficient at various chordwise locations. Figure 4 indicates that the pressure coefficient increases with increasing wedge angle over the forward region and over the rear region the pressure coefficient decreases with increasing wedge angle. Table II gives the analytical results for finite wedges in unbounded, incompressible streams ( $a/b = \infty$ ,  $M_0 = 0$ ).

The Euler numbers for the tunnel-wedge configurations were calculated by equations (15) and (18); the results are given as figure 5. The Euler numbers must tend to the values for infinite wedges as  $x/L \rightarrow 0$ ; these values may be calculated by equation (4). Only in a small region close to the leading edge does the Euler number approximate a constant value in the flow direction, even for this case of an unbounded stream. Thus, if an average Euler number be taken for each wedge angle in the range  $0 \leq x/L \leq 0.2$ , the deviation from this value is  $\pm 10$  percent at  $x/L = 0$  and  $x/L = 0.2$ , respectively. The solutions of the boundary layer equations given in references 4 to 6 and elsewhere assume a constant Euler number in flow direction, whereas figure 5 shows that a constant nonzero Euler number cannot be obtained with a finite wedge. It may be deduced, therefore, that for an experimental realization of an infinite wedge-type pressure gradient, it would be advisable to adjust the bounding walls of the tunnel to impose the proper pressure distribution on the test body.

Effect of tunnel-wedge ratio. - Pressure coefficients for various tunnel-wedge ratios ranging from about 1.10 to 2.8 for  $\theta = 20^\circ$  are given in figure 6(a) as a function of the chordwise location. To indicate better the influence of tunnel-wedge ratio, a cross plot of



figure 6(a) was made in figure 6(b). For decreasing values of  $a/b$  the pressure coefficient decreases for all  $x/L$  shown. The region of  $a/b$  where the influence on  $C_{p,i}$  is small is seen to be of the order of 100 or more, at least for the incompressible flow considered here. For the tunnel-wedge ratio of the current experiments,  $a/b = 2.8$ , the wall proximity has a decided influence on the pressure coefficient.

The effect of the tunnel-wedge ratio on the Euler number distribution for a  $20^\circ$  wedge is given in figure 7. The Euler number decreases with increasing tunnel-wedge ratio. The slope of the Euler number curve near the leading edge decreases quite markedly for appreciable tunnel-wedge ratios; hence conditions here more closely approximate those for an infinite wedge.

Heat transfer. - Predictions of heat transfer to a  $30^\circ$  wedge with a tunnel-wedge ratio of 2.83 were made using the methods of reference 7 for an impermeable wall with small temperature differences. The results are shown in figure 8, where  $Nu/\sqrt{Re_0}$  is plotted against the chordwise location. Curves 1, 2, and 4 show the effect of using different methods for heat-transfer prediction. Curves 2 and 3, which were obtained by the same heat-transfer method, show the effect of using different pressure distributions. The experimental pressure distribution for the test configuration will be given later. It should be emphasized that all the curves shown on figure 8 are theoretical, since no heat-transfer data were obtained in the present investigation.

Of the different heat-transfer methods utilized in figure 8, the equivalent wedge-type method is considered to be the best means of predicting heat-transfer results (ref. 7). Curve 2 in figure 8 will therefore be used as the criterion. A comparison of curves 1 and 2 shows that the equivalent infinite wedge and the equivalent wedge-type methods predict practically the same results for  $0 \leq x/L \leq 0.3$ , but as  $x/L$  increases from 0.3 the deviation between curves 1 and 2 becomes greater. Curve 4, calculated by the infinite wedge, constant Euler number method, differs from the criterion, curve 2, by 8 percent at  $x/L$  of 0.3 and 22 percent at 0.8. It may be concluded, therefore, that close to the leading edge of the body ( $x/L \approx 0.3$ ), use of either of the equivalent methods gives the same results, at least for the impermeable wall case. Aft of the leading-edge region, the equivalent wedge-type method should be used.

Curves 2 and 3, which use theoretical and experimental pressure distributions, respectively, and the equivalent-wedge type heat-transfer method show curve 3 deviating from curve 2 by about 6 percent at  $x/L$  of 0.3 and 9 percent at 0.8. This deviation is believed to be due mainly to the influence of separation on the experimental pressure distribution. For regions where separation is less influential ( $x/L \leq 0.3$ ), the use of the theoretical pressure distribution should be satisfactory if accuracies in heat-transfer predictions of the order of 5 percent are tolerable.

### Experimental

Flow visualization. - The results of the flow visualization studies for the test wedge at an upstream Mach number of 0.410 are shown in figure 9. The support rod and pressure leads on the wedge are also visible. To exhibit better the effect of the flow on the paint, figure 9(a) shows the wedge after painting before insertion in the tunnel. The photograph in figure 9(b) was taken after the visualization run was made and the dark traces of the hydrogen sulfide which emanated from the static-pressure taps may be seen. Note that the trace on the wall followed the wedge contour very well and there is no apparent tendency for any secondary flow. This is also borne out in the front view of the wedge in figure 9(c). Here it can also be seen that the flow causes the paint to form ridges (white) parallel to the side wall, confirming the two-dimensionality of the flow.

Pressure distribution. - The experimental pressure distributions obtained from the  $30^\circ$  wedge for a tunnel-wedge ratio of 2.8 are shown in figure 10 for different upstream Mach numbers along with the theoretical pressure coefficients obtained from equation (10) for  $M_0 = 0$  and from equation (21) for  $M_0 \neq 0$ . The trends of the experimental data regarding effects of chordwise location and compressibility on the pressure coefficient follow those predicted theoretically. The absolute values, however, are consistently greater than predicted. This effect is probably attributable to the influence of the trailing-edge separation on the wedge pressure distribution. Close to the leading edge, where the influence of separation should be small, the deviation between theory and experiment is relatively slight. Similar influences on the pressure distribution due to separation from cylindrical bodies are noted and discussed in reference 18.

From the experimental pressure coefficients  $C_p$  for the lowest test Mach number  $M_0 = 0.266$ , the incompressible pressure coefficients  $C_{p,i}$  may be calculated by the Kármán-Tsien method (eq. (21)). Then these values of  $C_{p,i}$  may be inserted in equation (21) and  $M_0$  assigned the value 0.464, and new pressure coefficients calculated for comparison with the data at this Mach number. The pressure coefficients so obtained are given by the dashed line in figure 10. It is seen that the dashed line yields smaller numerical values of  $C_p$  than the experimental data for  $M_0 = 0.464$ , probably because the Kármán-Tsien formula is strictly applicable only for an unbounded stream, whereas the proximity of the tunnel wall in the experiment increases the influence of compressibility.

The Kármán-Tsien formula corrects the pressure coefficient for disturbances caused by the body in the flow field. For the case of small

tunnel-wedge ratio, however, an additional correction is needed for the change in flow area. The effects of area change may be estimated by use of equation (3.26) of reference 14. Because the area change is of smaller order of magnitude than the disturbances for most investigations, a detailed examination of this method was not made for the present experiments.

Experimental Mach number distributions for various wedges are given in reference 1 for the transonic speed range and large tunnel-wedge ratios. Experimental pressure coefficients may be calculated from these data with equation (1b). For the tunnel-wedge ratios used in the experiments (see table II), theoretical pressure coefficients and chordwise locations may be computed for incompressible flow by equations (10) and (12) (bounded stream) and extended to compressible flow by equation (21); or, since the tunnel-wedge ratio is large, equation (17) (unbounded stream) may be used for the incompressible solution. Results of calculations using equations (10) and (12) are presented in figure 4. Theoretical pressure coefficients may also be calculated by equation (1c), the chordwise location then being given by equation (23) or (24) when the tabulated values of the Bessel functions in reference 15 are used. Hereinafter use of equations (10) and (12) (from Schwarz-Christoffel mapping theorem) in conjunction with equation (21) will be designated the mapping - KT (Kármán-Tsien) method; use of equation (22) will be defined as the linearized method; and use of equations (23) and (24) will be called the hodograph method.

The experimental pressure coefficients calculated from the results of reference 1 for wedge angles of  $9^\circ$  and  $15^\circ$  and an upstream Mach number of 0.824 are shown in figure 11(a). The point of zero pressure coefficient moves downstream with increasing wedge angle, as was shown analytically in figure 4(a). The experimental shift in chordwise location of this point due to an angle increase from  $9^\circ$  to  $15^\circ$  is about  $7\frac{1}{2}$  percent from figure 11(a), whereas the predicted shift from figure 4(a) would be about 7 percent. The locations of the points of zero pressure coefficient shown in figures 4(a) and 11(a) differ, however, because of the influence of upstream Mach number.

The experimental results for a wedge angle of  $20^\circ$  and an upstream Mach number of 0.700 are compared with the theoretical linearized, mapping-KT, and hodograph methods in figure 11(b). This figure indicates that the mapping-KT method agrees best with experiment for this wedge angle and upstream Mach number. It is to be expected that the mapping method would be better than the linearized method, since the mapping method considers the influence of the wedge angle on the pressure coefficient whereas the linearized method does not. The hodograph method, which provides the most accurate theoretical computation, should also

be in good agreement with experiment. The fact that the experimental values fall below those predicted by the hodograph method is possibly due to compensating effects involving the influence of viscosity and the subsequent formation of boundary layer. (A qualitative discussion of boundary layer influence on wedge pressure distribution is given in ref. 16.) The boundary layer would tend to make the experimental wedge act roughly as a wedge with a slightly larger angle than the geometric wedge, and from figure 4(a) it can be seen that this would tend to decrease the pressure coefficient over the rear part of the wedge. Since the mapping-KT method here predicts lower values of  $C_p$  than does the hodograph method, the experimental data are in somewhat better agreement with the mapping-KT method than with the hodograph method. It appears therefore that the mapping-KT method, which is easier to apply than the hodograph method, may be used to obtain wedge pressure distributions at least for  $M_0 \leq 0.7$  and  $\theta \leq 20^\circ$ .

Only the hodograph method, however, is in good agreement with experiment for Mach numbers close to unity, as may be seen in figure 11(c) for  $M_0 = 0.892$ . Near the leading edge, where the local Mach number is small, the mapping-KT and linearized methods are in good agreement with experiment. The hodograph method is lower than experiment because at the leading edge ( $M = 0$ ) the hodograph method yields  $C_p = 0.662$  by equation (1c). For the mapping-KT method,  $C_p = 1.378$  by equations (1a) and (21). A pressure coefficient of unity is obtained from equation (1b) by setting  $M = 0$  and using the first two terms of a

binomial expansion of  $\left(1 + \frac{\gamma-1}{2} M_0^2\right)^{\frac{\gamma}{\gamma-1}}$ . For the linearized method, equation (22),  $C_p$  is asymptotic to the ordinate at  $x/L = 0$ .

Aft of the leading-edge region, the linearized and mapping-KT methods do not properly predict the influence of the upstream Mach number. The hodograph method, on the other hand, is in good agreement with experiment over most of the wedge.

#### SUMMARY OF RESULTS

The results of an analytical and experimental investigation of the pressure distribution about wedges in bounded and unbounded subsonic streams are as follows:

1. The analytical solutions showed that, to properly estimate the wedge pressure coefficient, it is necessary to make a detailed examination of the flow with due consideration to the relative chordwise location, wedge angle, tunnel-wedge ratio, and upstream Mach number.

2. It was found from the analytical results for an unbounded stream that the region of applicability of the infinite wedge-type velocity distribution assumed in the solution of laminar boundary layer equations is approximated only within 10 percent for a limited region near the leading edge. For tunnel-wedge ratios of the order of 5 or less (bounded stream), the infinite wedge-type velocity distribution is realized only at the leading edge.

3. Predictions of heat transfer to a  $30^\circ$  wedge with small tunnel-wedge ratio (2.8) showed that use of the theoretical pressure distribution rather than of the experimental may be satisfactory if the desired accuracy in the heat transfer is of the order of 5 percent and the region is not markedly influenced by flow separation.

4. The experimental pressure coefficients for the two-dimensional flow over the  $30^\circ$  wedge with a tunnel-wedge ratio of 2.8 were not in good agreement with the theory for a finite wedge in a bounded stream, probably because of the influence of flow separation on the experimental results.

5. Comparison of previously published experimental results and theory in the high subsonic region for large tunnel-wedge ratios (greater than 100) indicated that the simple mapping Kármán-Tsien method was in good agreement with experiment for wedge angles from  $9^\circ$  to  $20^\circ$  and upstream Mach numbers to 0.700. For Mach numbers of the order of 0.900 and a wedge angle of  $20^\circ$ , the hodograph method was in better agreement with experiment than either the mapping or linearized methods.

Lewis Flight Propulsion Laboratory  
National Advisory Committee for Aeronautics  
Cleveland, Ohio, January 6, 1953

## APPENDIX - SYMBOLS

The following symbols are used in this report:

|                 |  |
|-----------------|--|
| A,B,C,D,<br>E,F | points on fig. 2   |
| a               | tunnel height  |
| b               | maximum wedge thickness  |
| $C_p$           | pressure coefficient, $C_p \equiv \frac{p - p_0}{\frac{\rho_0 U_0^2}{2}}$                  |
| c               | constant of proportionality, eq. (3)   |
| Eu              | Euler number, $Eu \equiv \frac{-x \frac{dp}{dx}}{\rho U^2}$                                |
| H               | heat-transfer coefficient  |
| h               | width of interval in finite difference integration, eq. (13)                               |
| $I_p$           | modified Bessel function of first kind of order p  |
| $K_p$           | modified Bessel function of second kind of order p   |
| k               | thermal conductivity   |
| L               | length of wedge surface  |
| l               | length of afterbody  |
| M               | Mach number, $U/\sqrt{\gamma RT}$  |
| m               | exponent in eq. (3)  |
| N               | function of Mach number, $N = 2/3 (1 - M^2)^{\frac{3}{2}}$                                 |
| Nu              | Nusselt number, $HL/k$   |
| n               | number of intervals advanced from initial value in finite difference integration, eq. (13) |

|                 |   |
|-----------------|---|
| p               | static pressure   |
| p'              | total pressure  |
| R               | gas constant  |
| Re <sub>0</sub> | Reynolds number, $\frac{U_0 \rho L}{\mu}$   |
| r               | summation index, eqs. (23) and (24)   |
| S               | constant in transformation for finite wedge in bounded stream, $S = \frac{a}{2\pi}$   |
| s               | constant in transformation for finite wedge in unbounded stream, eq. (16)   |
| T               | static temperature  |
| T'              | total temperature   |
| t               | constant in transformation for finite wedge in bounded stream, $t = \left( \frac{a/b}{a/b - 1} \right)^{\frac{2\pi}{\theta}}$ |
| U               | velocity  |
| v               | function of wedge angle, $v = \frac{\gamma+1}{2} \theta$  |
| w               | complex potential   |
| x               | distance along wedge surface measured from leading edge   |
| y               | spanwise distance on wedge surface  |
| z               | complex variable of physical plane  |
| $\alpha$        | real component of $\zeta$   |
| $\gamma$        | ratio of specific heats, $\gamma = 1.4$   |
| $\Delta$        | finite difference operator  |
| $\zeta$         | complex variable of transformed plane   |

$\theta$  wedge opening angle  
 $\mu$  absolute viscosity of fluid  
 $\rho$  density of fluid

Subscripts:

0 condition upstream of body  
 i incompressible  
 1 initial value in finite difference integration, eq. (13)  
 2, 3 real root  
 $\infty$  undisturbed region, upstream or downstream of wedge

REFERENCES

1. Bryson, Arthur Earl, Jr.: An Experimental Investigation of Transonic Flow Past Two-Dimensional Wedge and Circular-Arc Sections Using a Mach-Zehnder Interferometer. NACA TN 2560, 1951.
2. Pack, D. C.: Investigation of the Flow Past Finite Wedges of  $20^\circ$  and  $40^\circ$  Apex Angle at Subsonic and Supersonic Speeds, Using a Mach-Zehnder Interferometer. R.&M. No. 2321, British M.O.S., May 1946.
3. Cole, Julian D.: Drag of a Finite Wedge at High Subsonic Speeds. Jour. Math. and Phys., vol. 30, no. 2, July 1951, pp. 79-93.
4. Falkner, V. M., and Skan, Sylvia W.: Some Approximate Solutions of the Boundary Layer Equations. R.&M. No. 1314, Apr. 1930.
5. Brown, W. Byron, and Donoughe, Patrick L.: Tables of Exact Laminar-Boundary-Layer Solutions When the Wall is Porous and Fluid Properties are Variable. NACA TN 2479, 1951.
6. Brown, W. Byron, and Livingood, John N. B.: Solutions of Laminar-Boundary-Layer Equations Which Result in Specific-Weight-Flow Profiles Locally Exceeding Free-Stream Values. NACA TN 2800, 1952.
7. Eckert, E. R. G., and Livingood, John N. B.: Method for Calculation of Heat Transfer in Laminar Region of Air Flow Around Cylinders of Arbitrary Cross Section (Including Large Temperature Differences and Transpiration Cooling). NACA TN 2733, 1952.

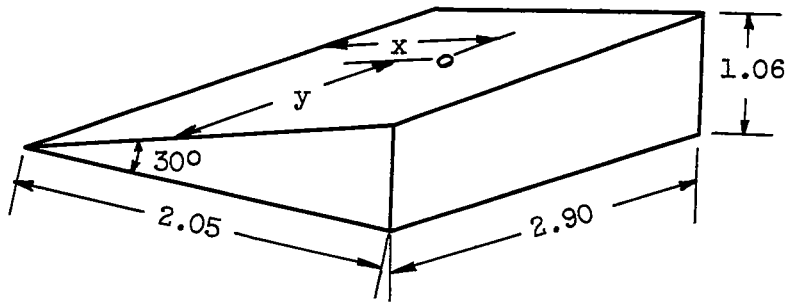




TABLE I. - GEOMETRY AND PRESSURE TAP LOCATIONS

FOR 30° WEDGE

[All dimensions are in inches.]



Pressure tap  
locations

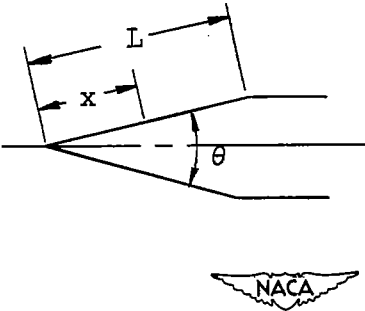
| y             | x    |
|---------------|------|
| Lower surface |      |
| 2.42          | 0.37 |
| 2.42          | .75  |
| 2.42          | 1.08 |
| 2.42          | 1.27 |
| 2.42          | 1.53 |
| 2.38          | 1.92 |
| 1.45          | .49  |
| 1.45          | .88  |
| 1.45          | 1.40 |
| 1.45          | 1.66 |
| .48           | .37  |
| .48           | .75  |
| .48           | 1.08 |
| .48           | 1.27 |
| .48           | 1.53 |
| .48           | 1.92 |
| Upper surface |      |
| 2.42          | 0.37 |
| 2.42          | .75  |
| 1.45          | .49  |
| 1.50          | .88  |
| .48           | .37  |
| .48           | .75  |



TABLE II. - THEORETICAL PRESSURE COEFFICIENTS FOR  
FINITE WEDGES IN UNBOUNDED, INCOMPRESSIBLE STREAMS

CALCULATED BY EQUATIONS (16) AND (17)

$$[a/b = \infty; M_0 = 0]$$

| $x/L$                             | $C_{p,i}$ |  |           |
|-----------------------------------|-----------|--|-----------|
| $\theta = 90^\circ; s/L = 0.5008$ |           |  |           |
| 0.0000                            | 1.0000    |  |           |
| .0338                             | .1595     |  |           |
| .0555                             | .1369     |  |           |
| .2651                             | .0535     |  |           |
| .4687                             | .0100     |  |           |
| .5189                             | .0000     |  |           |
| .5688                             | -.0100    |  |           |
| .7660                             | -.0566    |  |           |
| .9104                             | -.1162    |  |           |
| .9592                             | -.1586    |  |           |
| 1.0000                            | $-\infty$ |  |           |
| $x/L$                             | $C_{p,i}$ |  |           |
| $\theta = 15^\circ; s/L = 0.4997$ |           | $\theta = 20^\circ; s/L = 0.4986$  |           |
| 0.0000                            | 1.0000    | 0.0000   | 1.0000    |
| .0304                             | .2631     | .0385  | .3204     |
| .0591                             | .2175     | .0623  | .2790     |
| .2747                             | .0874     | .2830  | .1149     |
| .4800                             | .0165     | .4896  | .0221     |
| .5301                             | .0000     | .5397  | .0000     |
| .5799                             | -.0169    | .5892  | -.0225    |
| .7746                             | -.0958    | .7346  | -.0987    |
| .9150                             | -.2010    | .9189  | -.2764    |
| .9599                             | -.2780    | .9622  | -.3870    |
| 1.0000                            | $-\infty$ | 1.0000   | $-\infty$ |
| $\theta = 30^\circ; s/L = 0.4955$ |           | $\theta = 40^\circ; s/L = 0.4907$  |           |
| 0.0000                            | 1.0000    | 0.0000   | 1.0000    |
| .0367                             | .4570     | .0697  | .4928     |
| .0629                             | .3991     | .2611  | .2651     |
| .2994                             | .1673     | .4772  | .0862     |
| .4575                             | .0653     | .5775  | .0000     |
| .5583                             | .0000     | .7651  | -.2071    |
| .7499                             | -.1518    | .8932  | -.4704    |
| .8838                             | -.3352    | .9697  | -.9238    |
| .9661                             | -.6335    | 1.0000   | $-\infty$ |
| 1.0000                            | $-\infty$ |  |           |

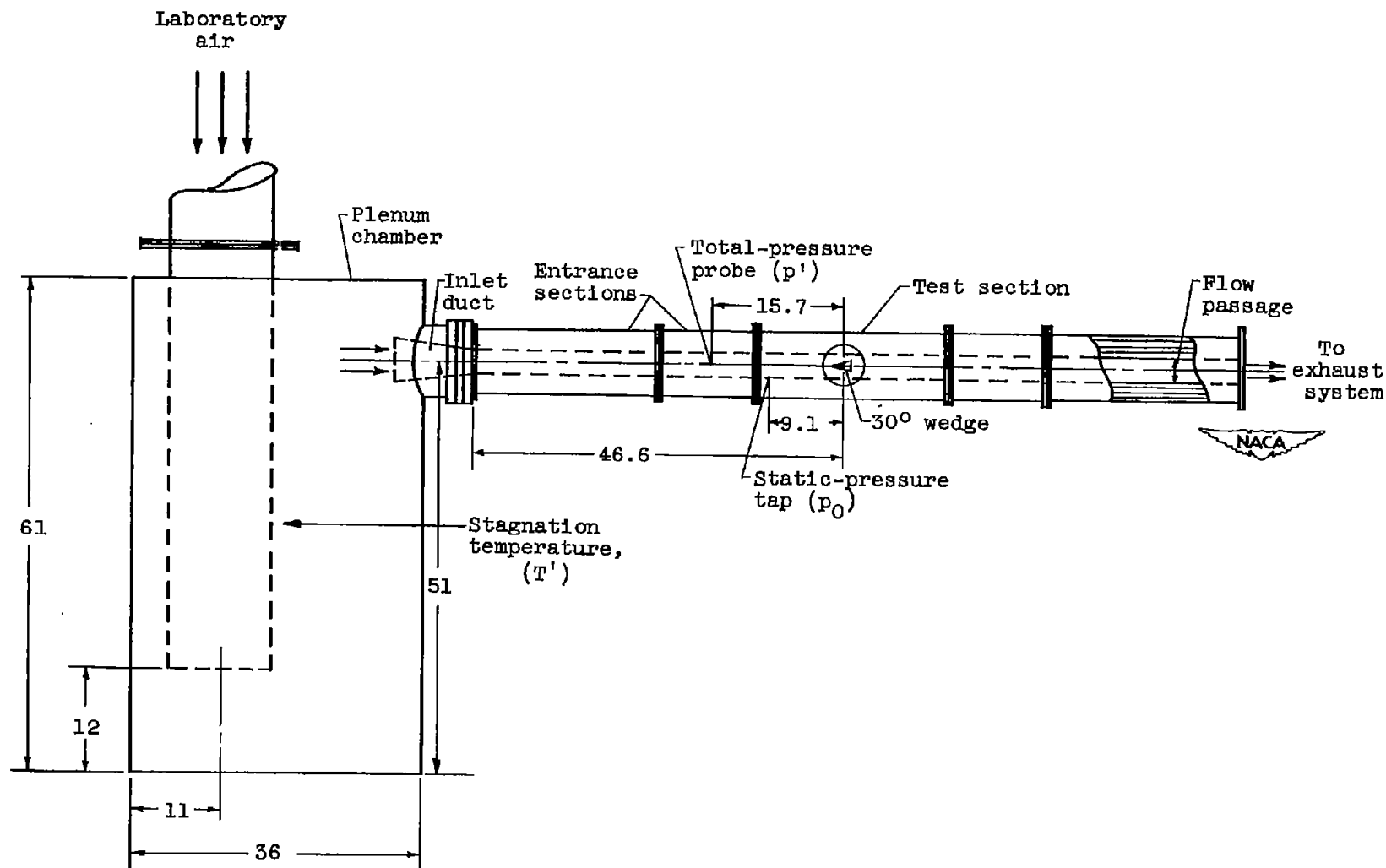


Figure 1. - Schematic diagram of test setup for 30° wedge. (All dimensions are in inches.)

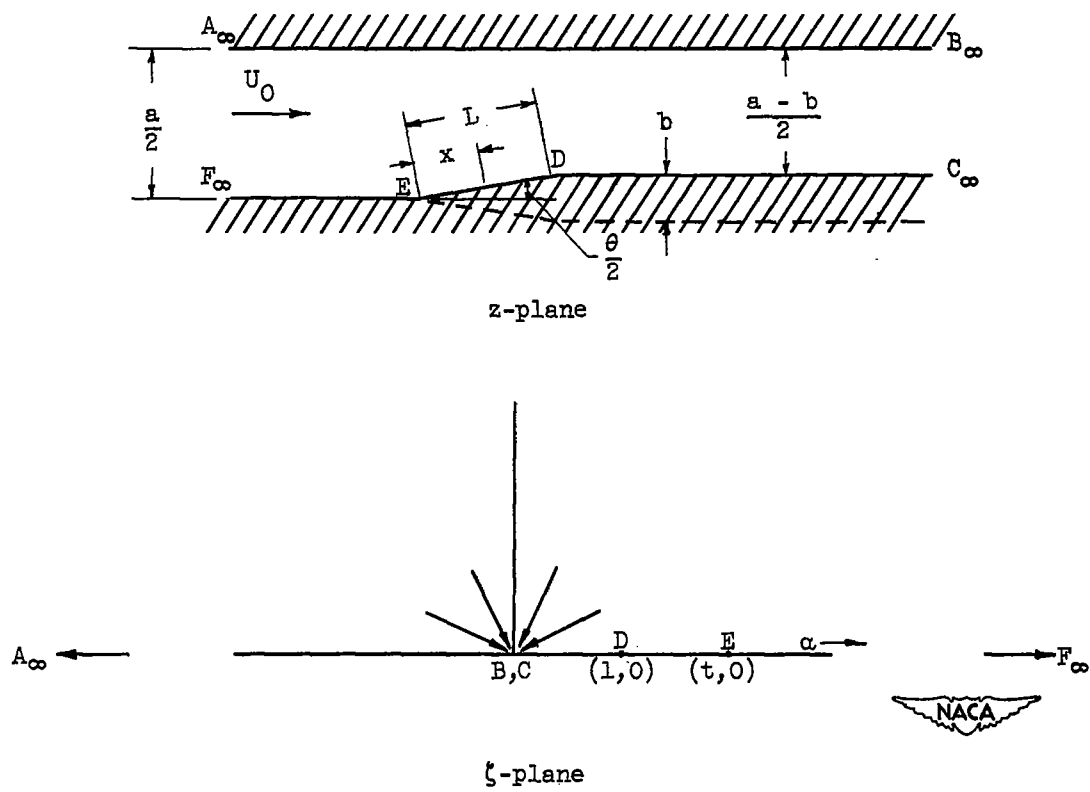


Figure 2. - Relation between physical and transformed planes for finite wedge in tunnel.

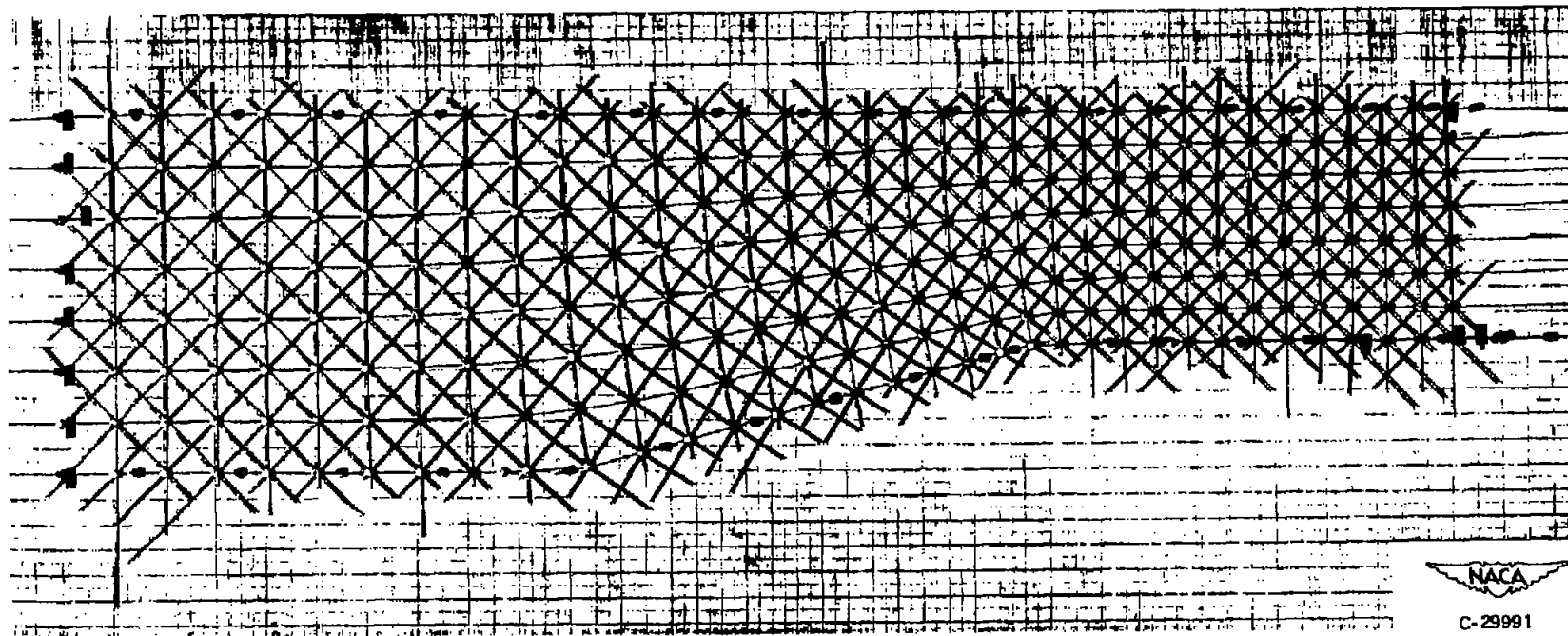
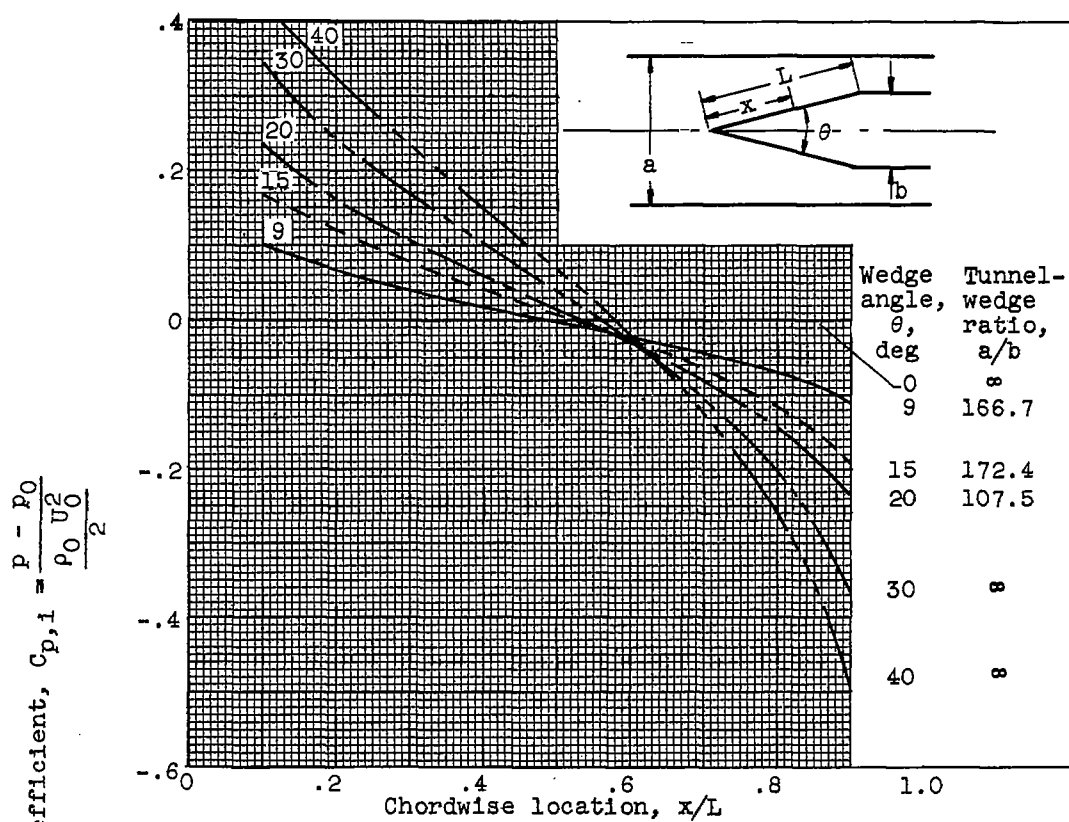
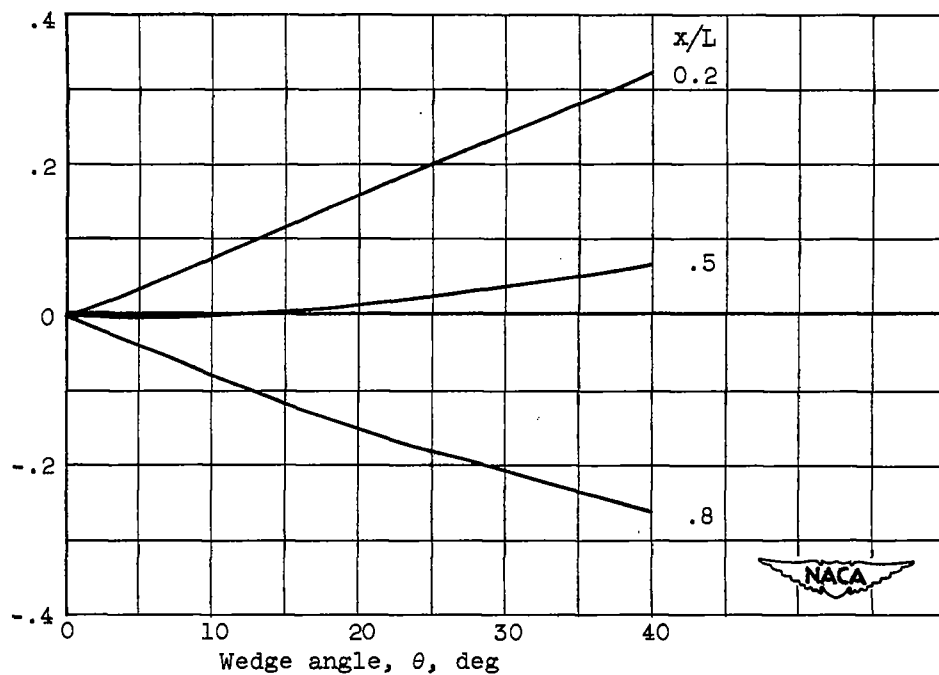


Figure 3. - Theoretical flow pattern obtained by wire mesh for wedge opening angle  $\theta$  of  $30^\circ$  and tunnel-wedge ratio  $a/b$  of 2.8.



(a) Computed pressure coefficient against chordwise location.



(b) Computed pressure coefficient against wedge angle.

Figure 4. - Influence of wedge angle on pressure distribution. Upstream Mach number, 0.

2805

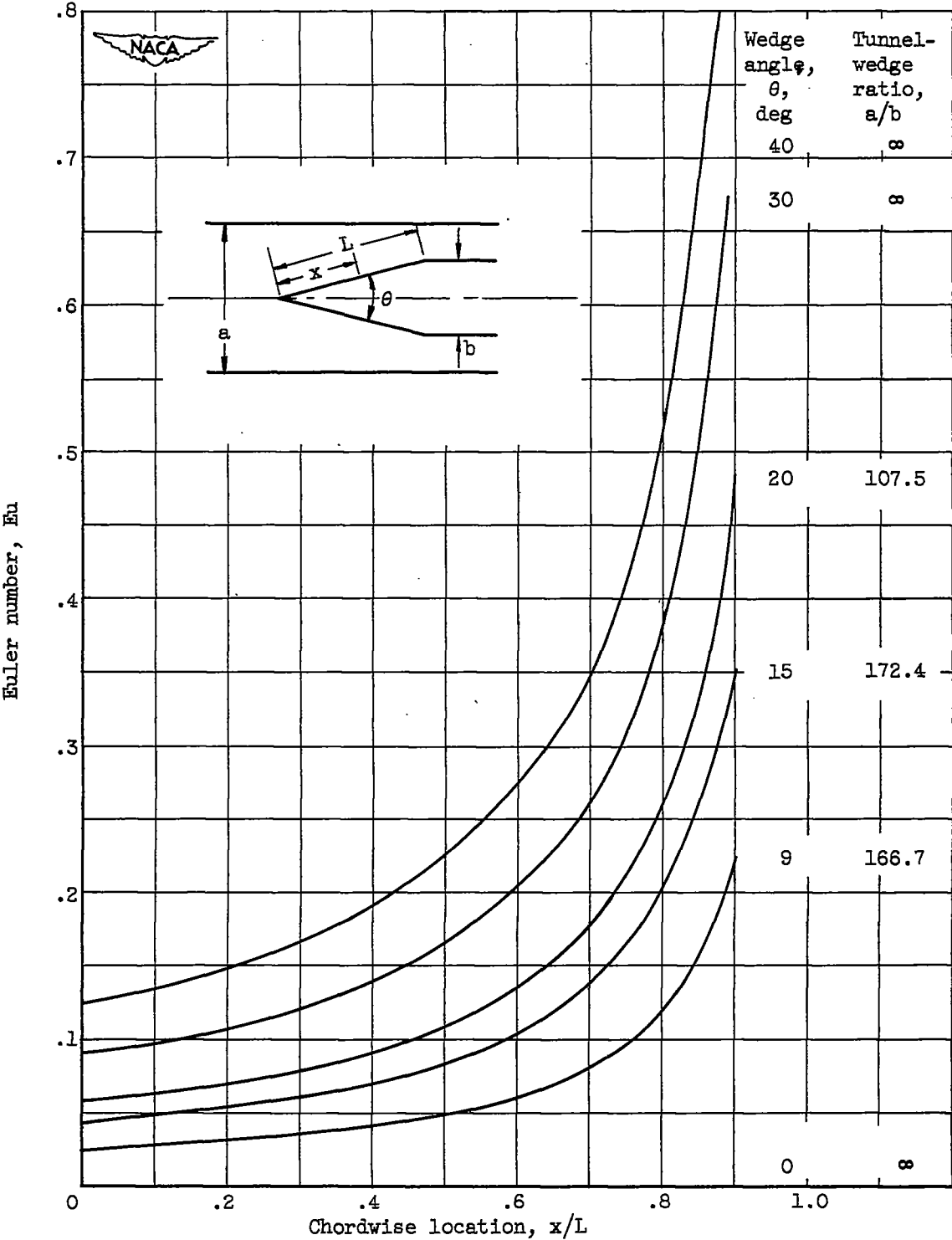
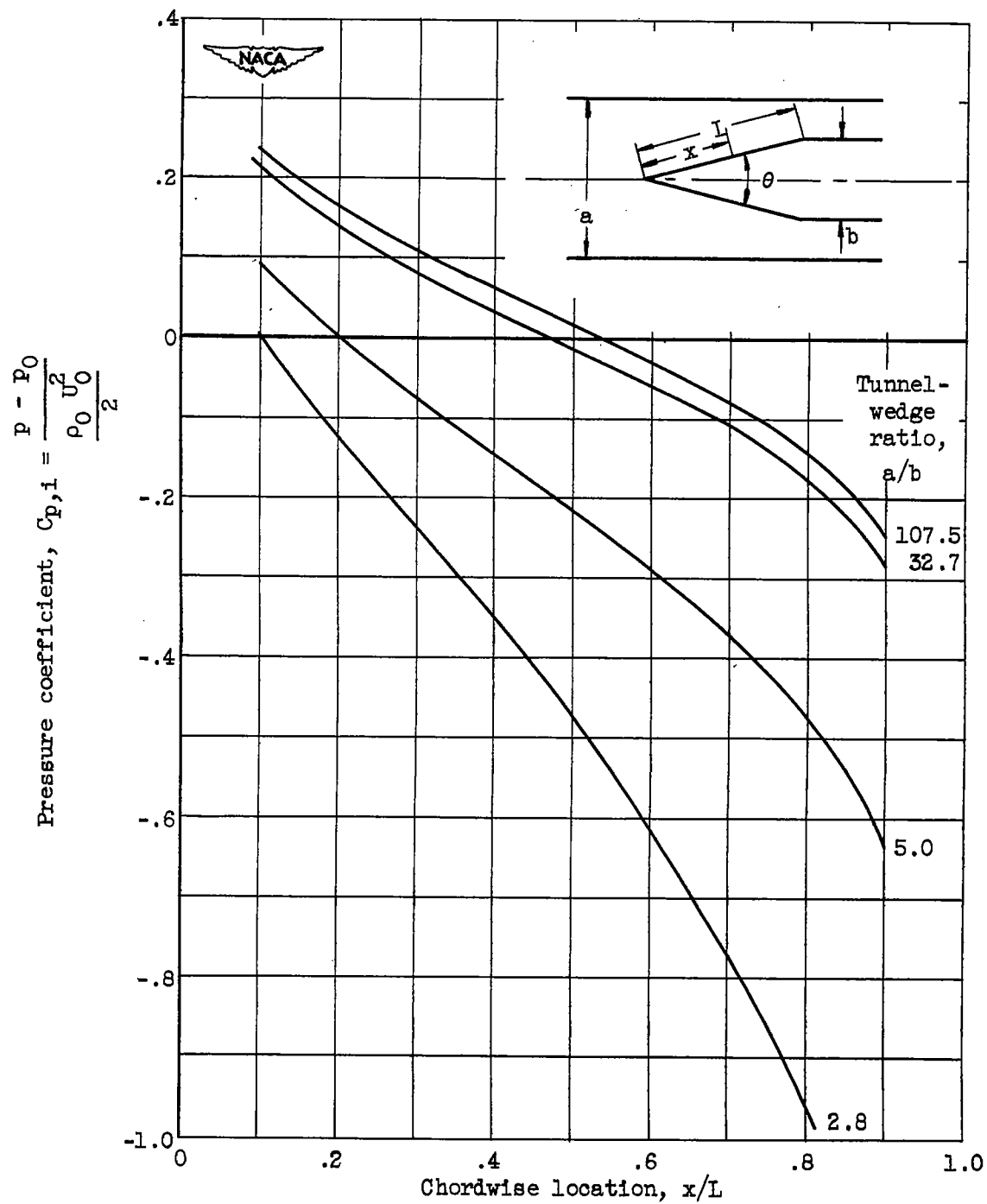


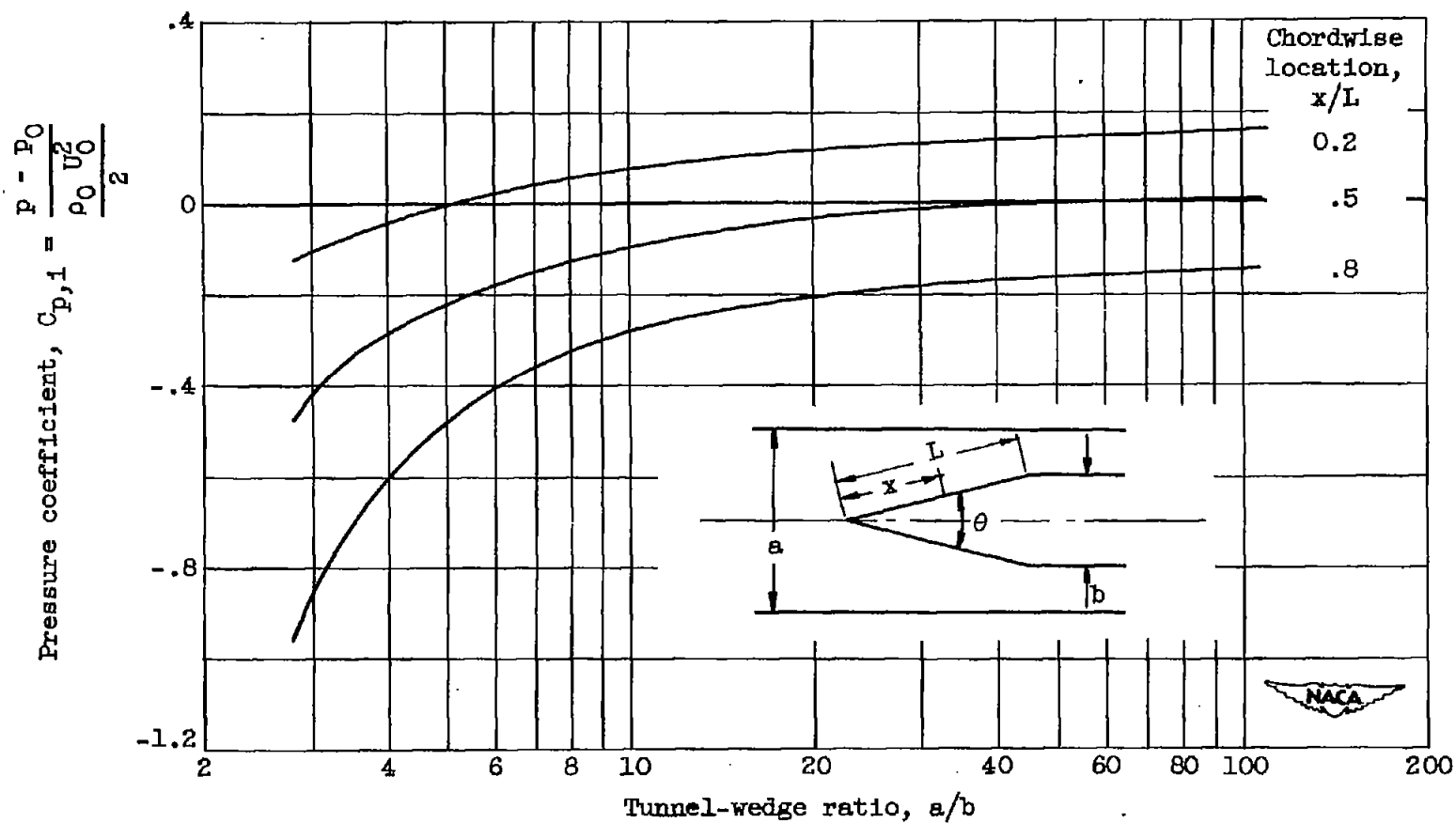
Figure 5. - Influence of wedge angle on Euler number distribution.  
Upstream Mach number, 0.





(a) Computed pressure coefficient against chordwise location.

Figure 6. - Influence of tunnel-wedge ratio on pressure distribution for  $20^\circ$  wedge. Upstream Mach number, 0.



(b) Computed pressure coefficient against tunnel-wedge ratio.

Figure 6. - Concluded. Influence of tunnel-wedge ratio on pressure distribution for  $20^\circ$  wedge. Upstream Mach number, 0.

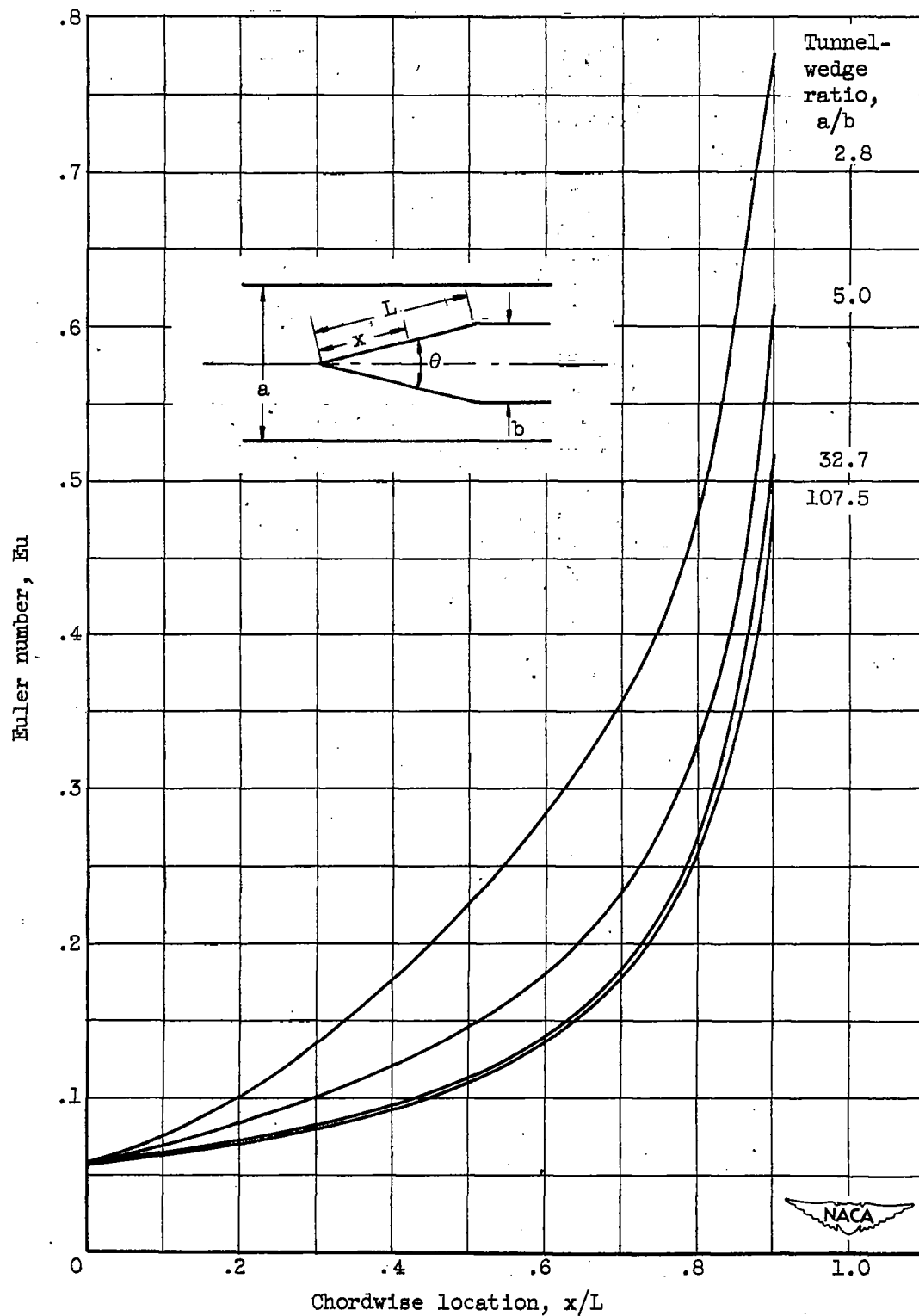


Figure 7. - Influence of tunnel-wedge ratio on Euler number distribution for  $20^\circ$  wedge. Upstream Mach number, 0.

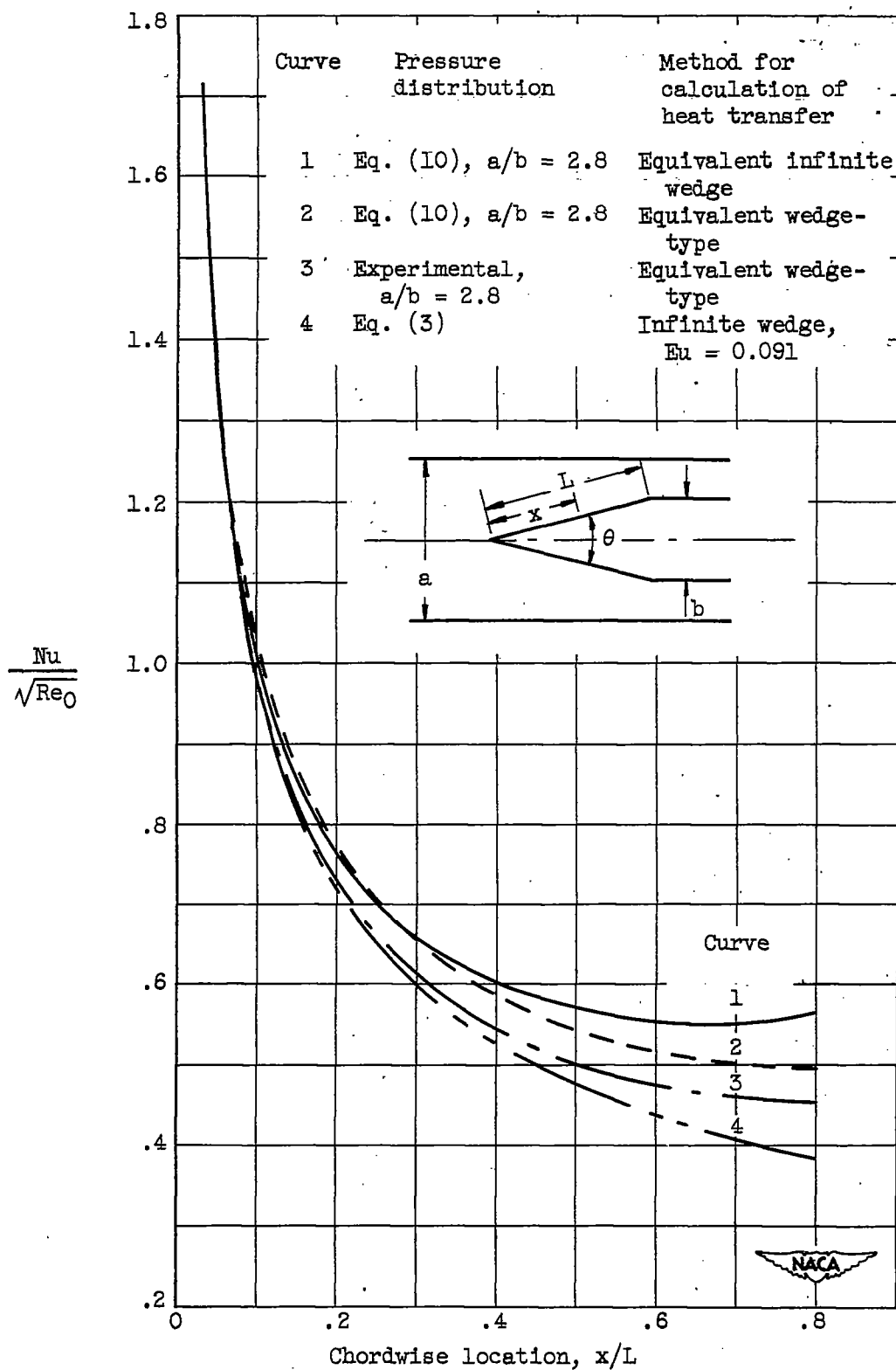
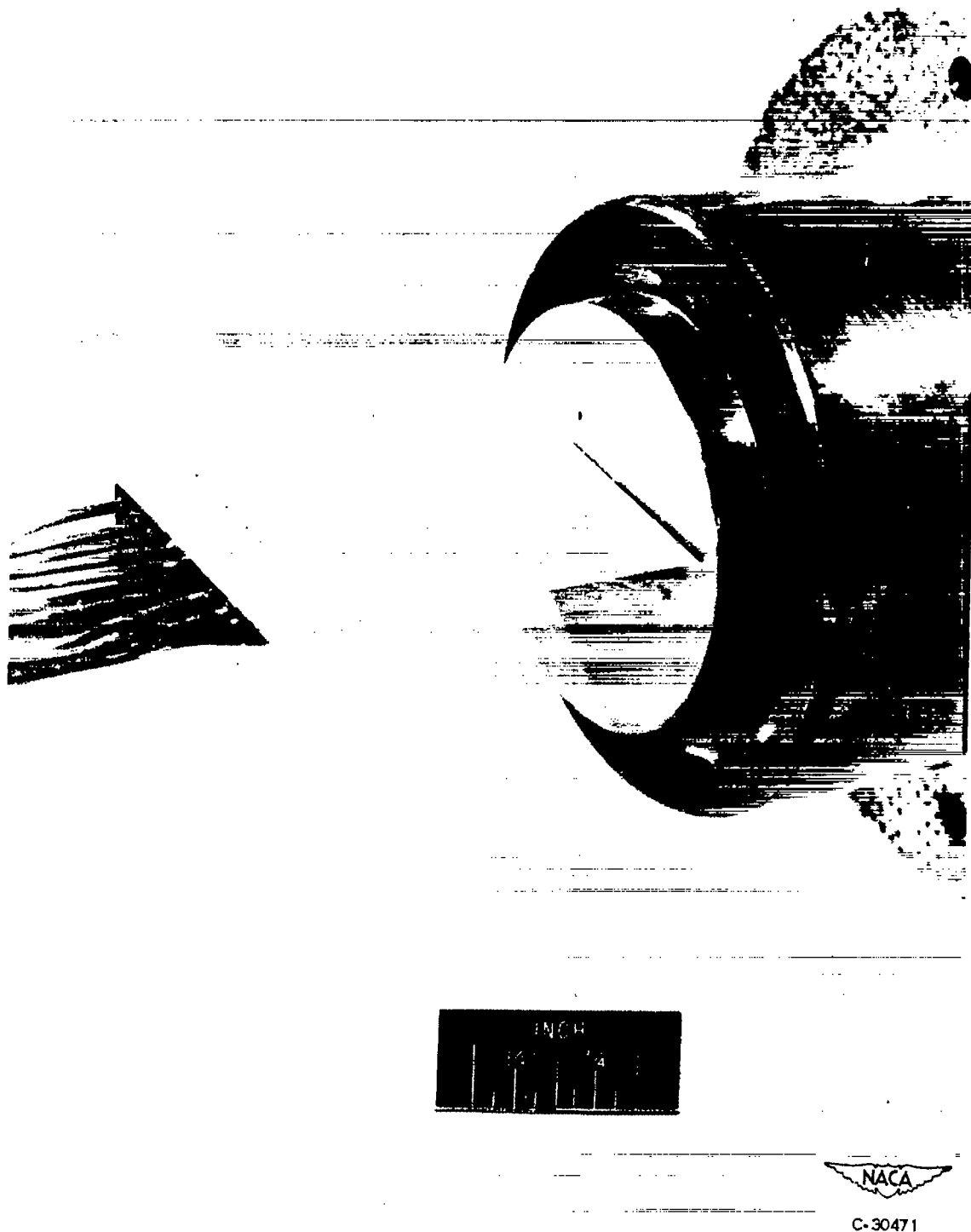
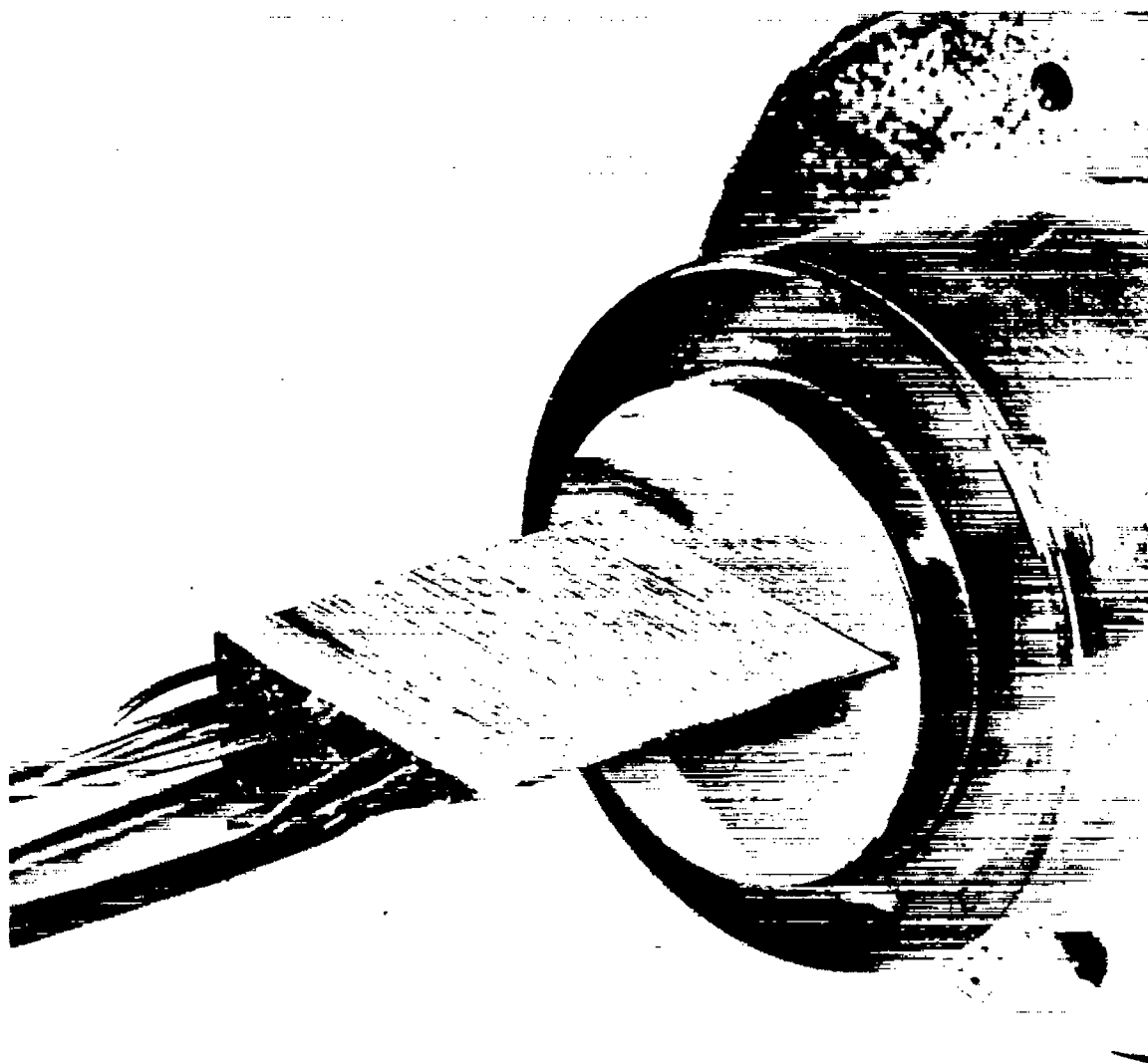


Figure 8. - Predicted heat transfer to  $30^\circ$  wedge.  
Upstream Mach number, 0.



(a) Painted wedge and side wall prior to subjection to air flow or hydrogen sulfide.  
Figure 9. - Results of flow visualization studies on 30° wedge with tunnel-wedge ratio of 2.8.

2805



(b) Hydrogen sulfide traces on wedge and side wall (side view).

Figure 9. - Continued. Results of flow visualization studies on 30° wedge with tunnel-wedge ratio of 2.8.



(c) Hydrogen sulfide and flow traces on wedge (front view).

Figure 9. - Concluded. Results of flow visualization studies on  $30^\circ$  wedge with tunnel-wedge ratio of 2.8.

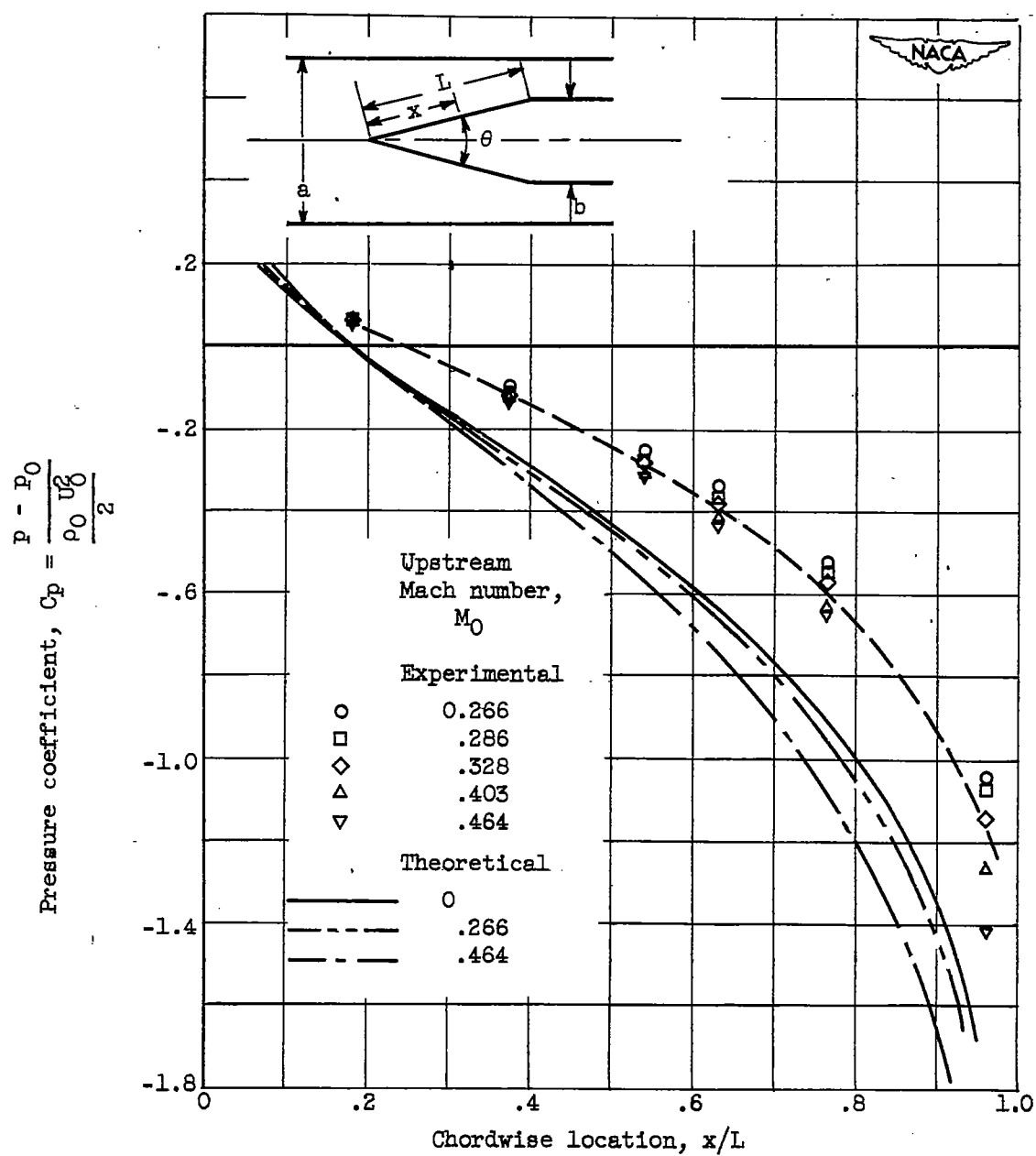
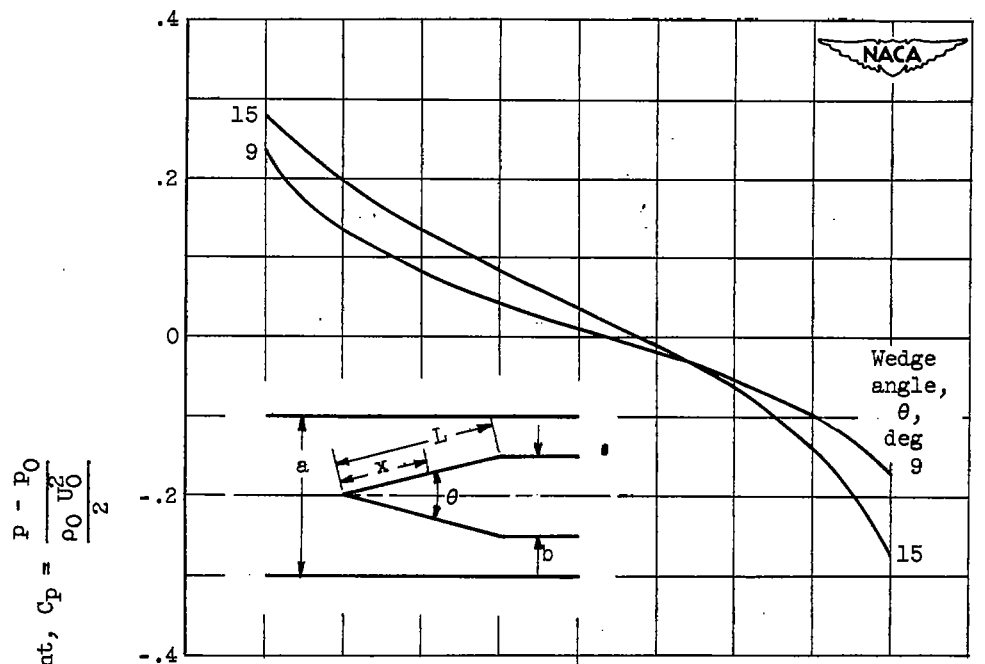
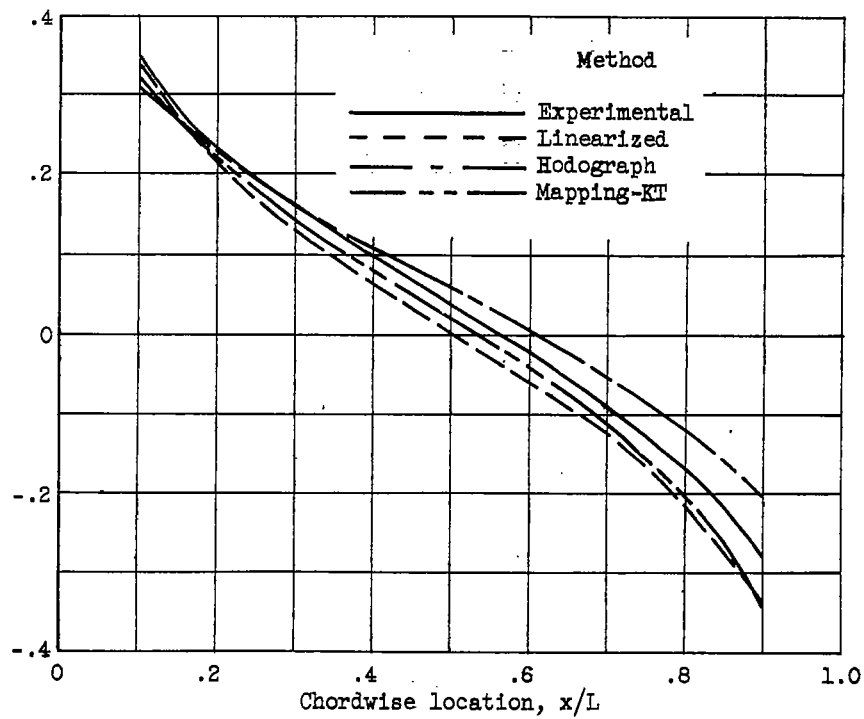


Figure 10. - Comparison of experimental and theoretical pressure coefficients for 30° wedge with tunnel-wedge ratio of 2.8.



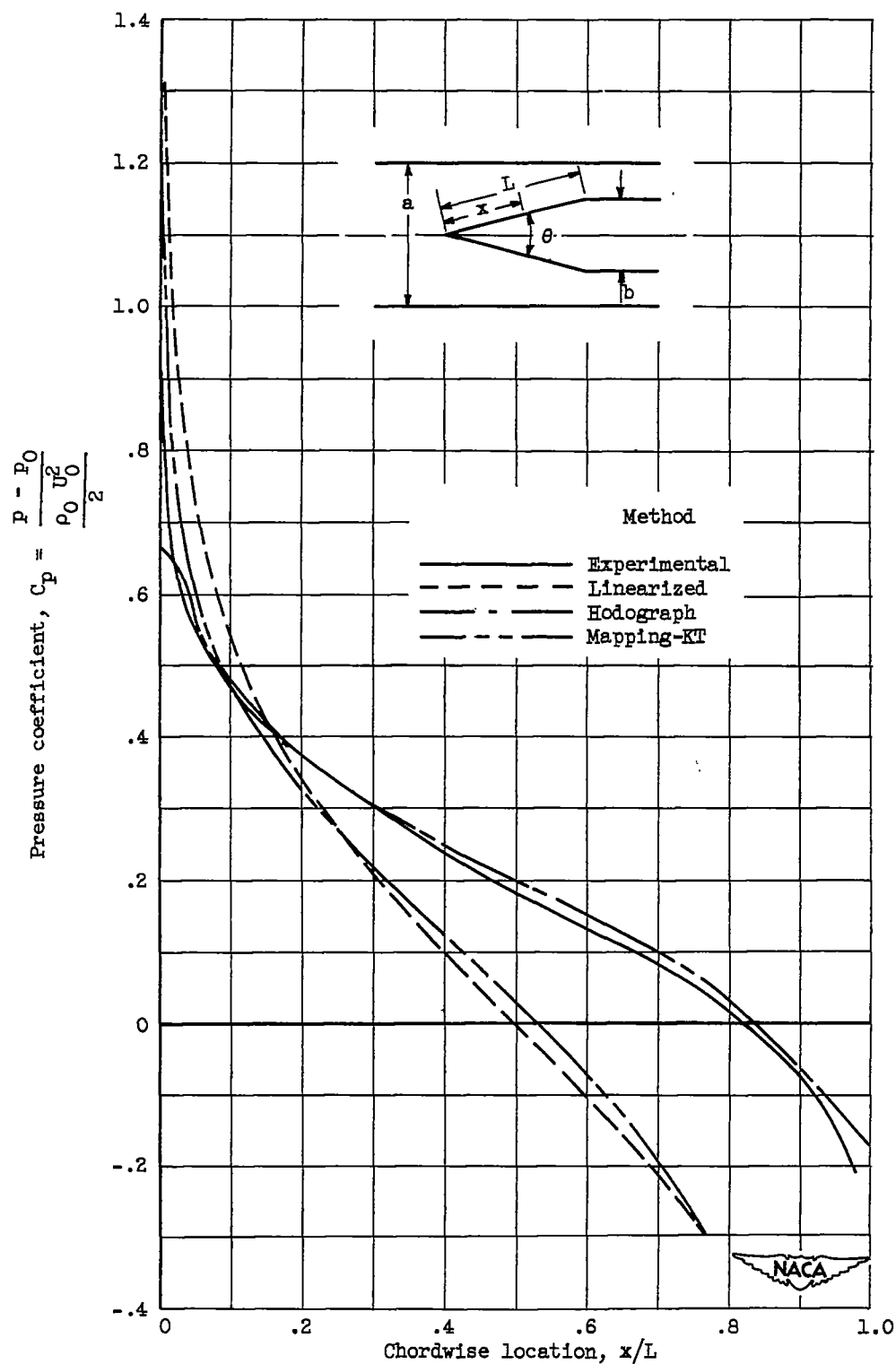


(a) Wedge angle,  $9^\circ$  and  $15^\circ$ ; upstream Mach number, 0.824.



(b) Wedge angle,  $20^\circ$ ; upstream Mach number, 0.700.

Figure 11. - Comparison of experiment with theory for large tunnel-wedge ratio ( $a/b > 100$ ).



(c) Wedge angle,  $20^\circ$ ; upstream Mach number, 0.892.

Figure 11. - Concluded. Comparison of experiment with theory for large tunnel-wedge ratio ( $a/b > 100$ ).